JOURNAL OF VIROLOGY, Feb. 2006, p. 1302–1310 Vol. 80, No. 3
0022-538X/06/$08.00+0 doi:10.1128/JVI.80.3.1302–1310.2006

Important Role for the Transmembrane Domain of Severe Acute Respiratory Syndrome Coronavirus Spike Protein during Entry

Rene Broer,[1]† Bertrand Boson,[2]† Willy Spaan,[1] François-Loïc Cosset,[2] and Jeroen Corver[1]*

Department of Medical Microbiology, Center of Infectious Diseases, Leiden University Medical Center, 2300 RC Leiden, The Netherlands,[1] and Laboratoire de Vectorologie Rétrovirale et Thérapie Génique, INSERM U412, IFR128 BioSciences Lyon-Gerland, Ecole Normale Supérieure de Lyon, 46 allée d'Italie, 69364 Lyon Cedex 07, France[2]

Received 3 June 2005/Accepted 11 November 2005

The spike protein (S) of severe acute respiratory syndrome coronavirus (SARS-CoV) is responsible for receptor binding and membrane fusion. It contains a highly conserved transmembrane domain that consists of three parts: an N-terminal tryptophan-rich domain, a central domain, and a cysteine-rich C-terminal domain. The cytoplasmic tail of S has previously been shown to be required for assembly. Here, the roles of the transmembrane and cytoplasmic domains of S in the infectivity and membrane fusion activity of SARS-CoV have been studied. SARS-CoV S-pseudotyped retrovirus (SARSpp) was used to measure S-mediated infectivity. In addition, the cell-cell fusion activity of S was monitored by a *Renilla* luciferase-based cell-cell fusion assay. $S_{VSV\text{-}Cyt}$, an S chimera with a cytoplasmic tail derived from vesicular stomatitis virus G protein (VSV-G), and $S_{MHV\text{-}TMDCyt}$, an S chimera with the cytoplasmic and transmembrane domains of mouse hepatitis virus, displayed wild-type-like activity in both assays. $S_{VSV\text{-}TMDCyt}$, a chimera with the cytoplasmic and transmembrane domains of VSV-G, was impaired in the SARSpp and cell-cell fusion assays, showing 3 to 25% activity compared to the wild type, depending on the assay and the cells used. Examination of the oligomeric state of the chimeric S proteins in SARSpp revealed that $S_{VSV\text{-}TMDCyt}$ trimers were less stable than wild-type S trimers, possibly explaining the lowered fusogenicity and infectivity.

In the winter of 2002 to 2003, a new type of pneumonia, severe acute respiratory syndrome (SARS), emerged in Guangdong province, China. The etiological agent causing this disease was found to be an unknown coronavirus, which was named SARS coronavirus (SARS-CoV) (10, 18, 23, 30).

Among the structural proteins of SARS-CoV, the spike (S) protein is the largest, comprising 1,255 amino acids. Research on SARS and other coronavirus S proteins has shown that S is involved in receptor binding and membrane fusion and is a major determinant of the immune response and pathogenesis (12). The spike protein is a type I membrane protein and is anchored in the membrane of the virion. Peplomers, oligomers of two or three spike proteins (9), form the distinctive "corona" on the virus.

The main receptor for SARS-CoV has been identified as angiotensin-converting enzyme 2 (ACE-2) (20). ACE-2 is expressed in several tissues, among which are epithelia in the lung and small intestine (15). It has been shown that amino acids 318 to 510 of SARS-CoV S are sufficient to bind to ACE-2 (1, 44, 45). L-SIGN has been shown to function as an alternative receptor, albeit with a significantly lower affinity than ACE-2 (17). Another lectin, DC-SIGN, has been implicated in enhancement of infection by dendritic cell transfer, a process earlier described for other viruses such as human immunodeficiency virus (HIV) and hepatitis C virus (HCV) (16, 24, 49).

In most but not all coronaviruses, S is cleaved during viral maturation by a host cell protease to create the subunits S1 and S2 (11, 40). It is unclear at this moment whether this type of cleavage of the SARS-CoV spike protein occurs. Recently, however, evidence has emerged showing that SARS S is cleaved during entry of the virus rather than during maturation. Low-pH-dependent, endosome-resident cysteine proteases (i.e., cathepsin L) have been shown to be involved in SARS-CoV entry by cleavage of S. Specific inhibitors of cathepsin L block entry of SARS pseudotypes and also infection with SARS-CoV (36).

Coronavirus S proteins have been proposed to be class I viral membrane fusion proteins (4). Class I proteins contain a fusion peptide at or close to the N terminus of the integral membrane fragment of the spike protein, consisting of about 20 hydrophobic amino acids, that enters the target membrane to initiate fusion. Furthermore, the class I proteins contain two 4,3-hydrophobic heptad repeats (HR) (6, 8) and often an aromatic-rich domain within or close to the transmembrane domain (TMD), which anchors the protein in the viral membrane.

The S2 subunit of the spike protein contains two heptad repeats (HR1 and HR2) with a high affinity for each other. HR1 is located downstream of the (internal) putative fusion peptide, and HR2 is located just upstream of the transmembrane domain (see Fig. 1a). Upon onset of fusion, a conformational change takes place in the spike oligomer, and the HRs form a so-called six-helix bundle—three α-helices formed by HR1 and three antiparallel HR2 α-helices—thus bringing the fusion peptide and the TMD of the spike protein in close proximity (4). This structure represents the "postfusion" con-

* Corresponding author. Mailing address: Leiden University Medical Center, Department of Medical Microbiology, E4-P, P.O. Box 9600, 2300 RC Leiden, The Netherlands. Phone: 31-715263649. Fax: 31-715266761. E-mail: j.corver@lumc.nl.

† R.B. and B.B. contributed equally to this work.

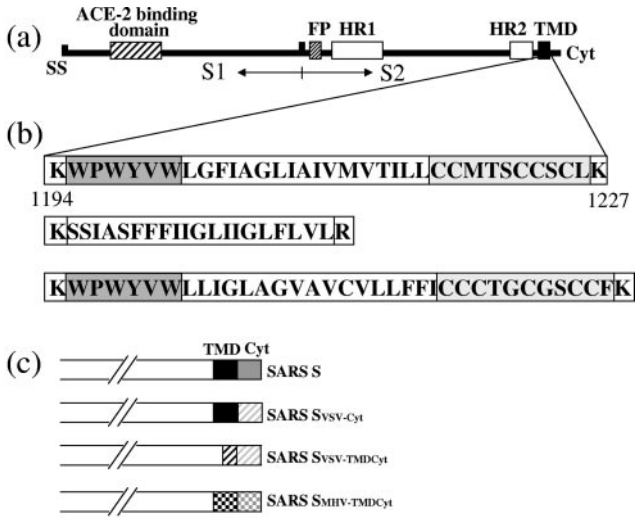

FIG. 1. Schematic presentation of the SARS-CoV spike protein. (a) The spike protein has an N-terminal signal sequence (SS), a putative fusion peptide (FP), two heptad repeats (HR), a transmembrane domain (TMD), and a C-terminal cytoplasmic domain (Cyt). The arbitrary border between S1 and S2 is indicated. The ACE-2 binding region is specified as part of S1. (b) Amino acid sequence of the transmembrane domain of SARS-CoV S (top), VSV-G (middle), and MHV S (bottom). The Trp-rich domain is depicted in a dark gray box, and the Cys-rich domain is light gray boxed. (c) Schematic representation of the wt S (S_{WT}) and S chimeras that are used in the experiments.

TABLE 1. Oligonucleotides used in this study

Name	Sequence
SAV027	CATCAACTGCATTGGGC
SAV031	ATATGAATTCGGATCCGCGGACGCGTA CCATGTTTATTTTCTTATTATTTCTTACTC
SAV032	ATATCTCGAGCATGCGGGCCCGGATCCCGG GTACCTTATGTGTAATGTAATTTGACACCC
SAV033	CTGAAACATCAAGCGAAAAGGC
SAV039	GATCCGGTACCCTCGAGC
SAV040	GATCGCTCGAGGGTACCG
SAV054	AATTGCATGCTCGAGAGGGGACGA TGTCAAGCTCTTCCTG
SAV055	AATTTCTAGAGGGCCCCTAAAAGG AGGTCTGAACATCATC
SAV058	CTACAGTACTGGAAAAGTTTG
SAV059	CAGTCCAATTGGATGCCTCC
SAV060	GGACGACTTCCTGACAGCTC
SAV061	CATACTGTGACCCCGCATCTC
SAV062	GATGGAGTACCGACTGGAGTCC
SAV065	GCATGACTAGTTGTTGCAGTTGCCTCC GAGTTGGTATCCATCTTTGC
SAV066	GGGGTACCGAGTTACTTTCCAAGTCGG
SAV067	AGTGTGCTAAATGATATCCTTTCGCG
SAV068	GATGCACAGAGAATATTCAAG
SAV069	CTTGAATATTCTCTGTGCATC
SAV070	GCAGTCTGCCATCCCACAGC
SAV071	GCTGTGGGATGGCAGACTGC
SAV072	GGGAAAATATGAGCAATATATTAAAAGCTC TATTGCCTCTTTTTTCTTTATCATAGGG

formation. The affinity of the two HRs for each other stabilizes this conformation and ensures fusion of the virus and target membrane. The trigger for this conformational change in the coronavirus spike protein is usually the interaction with the receptor (51). However, initiation of the membrane fusion process of SARS-CoV by low pH cannot be ruled out at this time (16, 49).

It is not known what conformational changes are occurring within the S protein to acquire the six-helix bundle. Since the native structure of the whole S protein has not been solved yet, in contrast to the HR1-HR2 complex (42, 47, 48), it remains unclear what other domains of S2 are involved in fusion. It has, however, become clear that, in contrast with other class I viral membrane fusion proteins, the N terminus of coronavirus S2 is not the fusion peptide, since it lacks the characteristic features described for fusion peptides. Rather, in coronaviruses the fusion peptide is an internal hydrophobic amino acid stretch. Putative coronavirus fusion peptides have been proposed (4) based on hydrophobicity plots and on peptide studies (32), but no conclusive evidence has been presented to date which points out the fusion peptide of coronaviruses.

Besides the HRs and the fusion peptide, another characteristic feature of the coronavirus S2 subunit is the length of its TMD. Although the exact borders of the TMD have never been experimentally identified, we assume that the TMD is located between the two charged lysine residues at amino acid positions 1194 and 1227 (see Fig. 1b). This means that the TMD would comprise 34 amino acids, which is longer than necessary to cross the membrane. Within the TMD there are three conserved, distinctive domains: an N-terminal tryptophan (Trp)-rich region, a hydrophobic central region, and a cysteine-rich C-terminal domain.

In this study, we set out to investigate the role of the unusually long TMD and the cytoplasmic tail of the spike protein in the membrane fusion activity and infectivity of SARS-CoV.

MATERIALS AND METHODS

Cells and viruses. 293T cells were obtained from the ATCC and cultured in Dulbecco's modified Eagle medium (DMEM) with 10% fetal calf serum (FCS). VeroE6R cells were a kind gift of A. D. M. E. Osterhaus, and they were cultured in DMEM with 10% FCS. SARS-CoV strain Frankfurt was a kind gift of H. F. Rabenau and H. W. Doerr.

Construction of SARS spike expression vectors. The SARS spike gene of the Frankfurt-1 isolate was cloned by reverse transcriptase PCR (RT-PCR) on RNA isolated from infected Vero cells as previously described (38) and cloned into the gateway vector pDEST-14 (Invitrogen). The gateway construct was completely sequenced and used as a basis for further cloning. The T7-driven SARS spike expression vector pLSS3 was obtained by cloning the 5′ end of the SARS spike gene into vector pL1A (38) after RT-PCR on isolated viral RNA using primers SAV31 and SAV033, located downstream of the unique NcoI site, resulting into construct pLSS1. (Sequences of primers used in this study are given in Table 1.) The 3′ end of the SARS spike gene was cloned into vector pLSS1 after RT-PCR with primers SAV032 and SAV027, located upstream of the unique EcoRV site, resulting in vector pLSS2. The internal NcoI-EcoRV SARS spike fragment from the gateway clone was cloned into vector pLSS2, leading to the full-length spike expression construct pLSS3. Construct phCMV-S_{WT} was made by first modifying vector phCMV (27) by insertion of a BamHI-KpnI-XhoI linker (SAV039/SAV040), leading to vector phCMV(BKX). The SARS spike gene was inserted into vector phCMV(BKX) in a 3-point ligation containing the BamHI-BlnI and BlnI-XhoI fragments from pLSS33, leading to vector phCMV-S_{WT}. Once cloned, the sequences of the 5′ and 3′ borders of the S-encoding region were verified.

Construction of other vectors. A cDNA clone containing ACE-2 cDNA was obtained from the German Resource Center for Genome Research (clone IRAKp961I1334Q2). PCR on this plasmid was carried out using primers SAV054 and SAV055. The PCR fragment was cloned into pcDNA3 using the introduced XbaI and XhoI sites. Sequencing of this clone using primers SAV054-SAV062 showed two point mutations. They were restored back to wild type by QuikChange mutagenesis (Stratagene) using primers SAV068-SAV071, yielding

pcDNA3/FLACE2. Subsequently, the T7 promoter of the plasmid was deleted by SpeI digestion and self-ligation (pcDNA3/FLACE2ΔSpeI). Then a cassette containing a T7 promoter, the *Renilla* luciferase gene, the 3′ nontranslated region (NTR) of hepatitis C virus, and a T7 termination signal (the fragment was originally obtained from plasmid pHCVwt-RLuc-3′UTR [C. B. E. M. Reusken, personal communication]) was cloned into this plasmid using the NotI and XhoI sites, yielding plasmid pFLACE2/T7rLuc.

Plasmid pBP9/CMVT7 contains a cytomegalovirus (CMV) promoter-driven T7 polymerase gene (7) followed by a simian virus 40 polyadenylation signal and was cloned using conventional cloning procedures.

Recombinant SARS spike expression. VeroE6R cells were seeded into 35-mm wells (0.5×10^6 cells/well) and 16 h later transfected with 2 μg of DNA per 35-mm plate using Lipofectamine (Invitrogen) according to the manufacturer's protocol. A typical labeling experiment was performed as follows. Cells were starved 18 h posttransfection (hpt) for 30 min in RPMI 1640 without Met and Cys and were subsequently labeled metabolically with RPMI 1640 without Met and Cys plus [^{35}S]Cys and [^{35}S]Met (ICN Biomedicals Inc.). After a 2-h labeling, the medium was removed and replaced by chase medium (DMEM plus 10% FCS and extra [2.5-fold] Met and Cys). Cells were lysed in RIPA buffer (3) after a chase period of 0, 3, 5, or 7 h. The lysates were centrifuged for 5 min at 13,000 rpm to remove nuclei and cell debris. Immunoprecipitations were performed on the supernatants as previously described (3) by using a polyclonal rabbit antibody against SARS-CoV kindly provided by M. Niedrig (16). Protein samples were EndoH digested according to the manufacturer's protocol (New England Biolabs) and analyzed on 8% polyacrylamide gels.

Biotinylation of spike proteins. 293T cells were transfected with a spike-encoding plasmid. At 24 h posttransfection, the cells were trypsinized and pelleted. After three washes with phosphate-buffered saline (PBS), cells were incubated in PBS plus 0.5 mg/ml Sulfo-NHS-LC-biotin (Pierce) for 20 min at 4°C. Subsequently, the cells were washed with PBS plus 0.1 M glycine and incubated in the same buffer for 15 min at 4°C. Cells were then washed twice with PBS and finally lysed in TENT buffer (50 mM Tris, pH 7.5, 5 mM EDTA, 150 mM NaCl, 0.5% Triton X-100).

Construction of spike chimeras. Chimeras $S_{VSV\text{-}Cyt}$ and $S_{VSV\text{-}TMDCyt}$ were made by fusion PCR. Fusion primer SAV065, 3′ primer SAV066, and 5′ primer SAV067 were used for $S_{VSV\text{-}Cyt}$. Fusion primer SAV072, 3′ primer SAV066, and 5′ primer SAV067 were used for $S_{VSV\text{-}TMDCyt}$. PCR products were digested with EcoRV and KpnI and inserted into vector phCMV-S_{WT}. Chimera $S_{MHV\text{-}TMDCyt}$ was made by replacing the StyI-BamHI fragment from vector pSP72-SS-EV-X (containing the SARS spike EcoRV-XhoI fragment of phCMV-S_{WT}) by the homologous fragment from mouse hepatitis virus (MHV) spike vector pTUGM-S (43), resulting in shuttle vector pSP72-$S_{MHV\text{-}TMDCyt}$-EV-X. The MHV sequence was introduced into vector phCMV-S_{WT} by exchanging EcoRV-XhoI fragments with pSP72-$S_{MHV\text{-}TMDCyt}$-EV-X.

Synthesis of SARS CoV-pseudotyped MLV particles (SARSpp). SARS spike murine leukemia virus (MLV) retrovirus particles were produced as described for HCVpp (2). Briefly, 293T cells were transfected using a $CaCl_2$ transfection kit (Clontech) with a set of retrovirus Gag and Pol expression constructs, a green fluorescent protein (GFP) reporter plasmid, and the SARS-CoV spike chimeras to be expressed. Supernatants were harvested 2 days after transfection and used to transduce VeroE6R cells. The percentage of GFP-positive cells was determined by fluorescence-activated cell sorter (FACS) analysis 4 days after transduction. A C-type reverse transcriptase activity kit (Innovagen, Sweden) was used to correct for the amount of retrovirus particles per ml of supernatant between transfections.

FACS analysis. Transduced VeroE6R cells (M6) were washed with PBS and harvested using trypsin. Cell were diluted in DMEM plus 10% FCS and pelleted for 5 min at $250 \times g$.

Cell pellets were washed in PBS and repelleted for 5 min at $250 \times g$. Cells were then resuspended in a final volume of 2.0 ml PBS. The percentage of GFP-positive cells was determined on a FACSCalibur (Becton Dickinson).

MLV SARS spike pseudoparticle neutralization assay. A total of 1×10^4 to 2×10^4 cells were incubated with 50-fold dilutions of human SARS-CoV sera (a kind gift of M. Niedrig, Robert Koch Institute) for 45 min at room temperature prior to infection of VeroE6R cells. Subsequently, infection was performed as described above.

Transduction of cells with SARSpp and titer determination. Retrovirus SARSpp supernatants were used to transduce target cells. Briefly, 2×10^5 cells were seeded 1 day prior to transduction in M6 wells. Equal amounts of SARSpp, as determined by a reverse transcriptase enzyme-linked immunosorbent assay, were used to transduce cells in a final volume of 600 μl in DMEM containing 4 μg/ml Polybrene. Medium containing SARSpp was replenished after overnight incubation with normal growth medium. Cells were harvested 3 to 4 days after transduction and the percentage of GFP-positive cells determined by FACS analysis.

Cell-cell fusion assay. One pool of 293T cells was transfected with pFLACE2/T7rLuc, and another pool was transfected with phCMV-S_{WT} (or an S chimera) and pBp9/CMVT7 using Lipofectamine 2000 (Invitrogen) using the manufacturer's protocol. After 17 to 20 h of incubation at 37°C, both pools of cells were trypsinized and mixed in equal amounts. After another 24-h incubation at 37°C, cells were lysed according to the manual of the *Renilla* luciferase assay system (Promega). Luciferase activity was measured using a luminometer (TD −20/20; Turner Designs). On the remainder of the cell lysate a Bradford assay was performed, to measure the protein concentration. Relative *Renilla* luciferase activity was calculated as the measured value divided by the protein concentration minus the measured value of the control (no S) divided by the protein concentration.

Determination of the oligomeric state of spike present on SARSpp. ^{35}S-labeled SARSpp retrovirus supernatants were purified with a 20% sucrose cushion (SW41 rotor, 2 h, 25 krpm). Pellets containing SARSpp were resuspended in PBS. Prior to immunoprecipitation, 1% sodium dodecyl sulfate (SDS) was added to the samples to solubilize the SARSpp. Immunoprecipitations were performed as previously described, using an anti-SARS-CoV polyclonal antiserum. Immunoprecipitates were resuspended in Laemmli loading buffer (19) without dithiothreitol and kept at room temperature or incubated 5 min at 80°C prior to loading of the samples on a 4% polyacrylamide gel.

RESULTS

Expression of SARS-CoV (Frankfurt) S protein and chimeras. The SARS-CoV (strain Frankfurt) S protein-encoding sequence was cloned into phCMV, yielding phCMV-S_{WT}. In addition, several chimeras were constructed to investigate the role of the TMD and the cytoplasmic domain of S in membrane fusion activity and infectivity. In chimera $S_{VSV\text{-}Cyt}$, the cytoplasmic tail of SARS-CoV S was replaced by its vesicular stomatitis virus G protein (VSV-G) counterpart. In $S_{VSV\text{-}TMDCyt}$, the transmembrane and cytoplasmic domains of SARS-CoV S were replaced by the VSV-G transmembrane and cytoplasmic domains. In $S_{MHV\text{-}TMDCyt}$, the transmembrane and cytoplasmic domains of SARS-CoV S were replaced by the MHV-A59 S transmembrane and cytoplasmic domains (see Fig. 1c).

First, expression and maturation of wild-type (wt) S and the S chimeras was studied. After transfection of VeroE6R cells with the proper plasmids, pulse-chase labeling was carried out. Cell lysates were subjected to immunoprecipitation with an S-specific antibody and subsequent EndoH digestion to check the maturation. At the start of the chase (Fig. 2a, lanes 0), the majority of wt S and S chimeras was EndoH sensitive (bands marked S_{Sens}), indicating that most of the S proteins had not passed the endoplasmic reticulum. However, a small portion of all S variants already had become EndoH resistant (bands marked S_{Res}) during the 2-h pulse, indicating that a fraction of S and the chimeras already was transported to the Golgi complex or further downstream the exocytosis route (compare lanes − and + EndoH). After a 7-h chase, the majority of S and the chimeras had become EndoH resistant. In summary, the expression and maturation of the S chimeras displayed the same kinetics as wt S protein. As a negative control, VSV-G was expressed from the same plasmid, resulting in only background bands in the gel when S-specific antibodies were used.

Transport of S and the S chimeras to the plasma membrane was confirmed by a biotinylation experiment. Surface proteins of S-transfected 293T cells were biotinylated, and cell lysates were subjected to immunoprecipitation with anti-S antibody. Subsequently, Western-blot analysis was carried out using

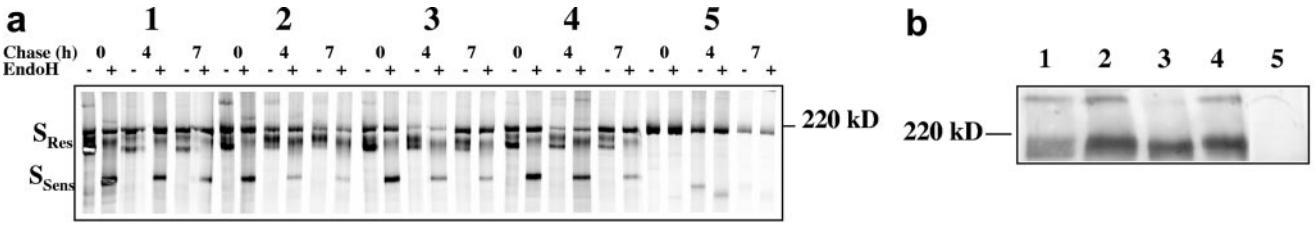

FIG. 2. Expression and maturation of S and S chimeras. (a) CMV-driven S expression plasmids were transfected into VeroE6R cells. After a 24-h incubation, cells were pulsed for 2 h with [^{35}S]Met-Cys and chased for the indicated periods (in hours). After the chase, cells were lysed and the S proteins were immunoprecipitated with anti-SARS serum. Samples were analyzed on an 8% PAA gel. Endo H-resistant S (S_{Res}) and EndoH-sensitive S (S_{Sens}) are indicated. Lanes: 1, S_{WT}; 2, $S_{VSV\text{-}Cyt}$; 3, $S_{VSV\text{-}TMDCyt}$; 4, $S_{MHV\text{-}TMDCyt}$; 5, VSV-G. (b) Cell surface expression of S was demonstrated by biotinylation of S proteins. Transfected 293T cells were incubated with sulfo-NHS-LC-biotin 24 h posttransfection. Subsequently, S-specific immunoprecipitation was carried out, followed by Western blot analysis using HRP-conjugated streptavidin. Bands were visualized by chemiluminescence. S-specific bands are indicated. Lanes: 1, S_{WT}; 2, $S_{VSV\text{-}Cyt}$; 3, $S_{VSV\text{-}TMDCyt}$; 4, $S_{MHV\text{-}TMDCyt}$; 5, mock.

horseradish peroxidase (HRP)-conjugated streptavidin. Figure 2b shows that the S chimeras were biotinylated at least to the same extent as wt S (S_{WT}), indicating that the S chimeras were transported to the plasma membrane in the same manner as the wt S protein.

Synthesis and characterization of SARS-CoV pseudotyped retrovirus. Next, we wanted to investigate the potential of S and the chimeras to mediate the infection of a cell. To do this, a SARS pseudotype system based on the retrovirus MLV was used. SARSpp were analyzed for their ability to transduce permissive VeroE6R cells. Since the particles contain a GFP-encoding RNA, the number of transduced cells could be measured by FACS analysis. Titers of 10^5 to 10^6 were reached, depending on the infection method (with or without spinoculation) (see Fig. 3a). Control particles, pseudotyped with RD114, the envelope of a feline endogenous retrovirus, reached titers of 10^6 to 10^7. To check whether the infectivity of the SARSpp was dependent on the SARS-CoV S protein, a neutralization assay was done with sera of several SARS patients, a SARS-specific rabbit serum, and control sera. Figure 3b shows that the infectivity of the SARSpp was specifically inhibited by the SARS patient sera and the S-specific polyclonal rabbit serum. This indicates that the infectivity of the SARSpp was dependent on SARS-CoV S and that the S protein was fully functional in the SARSpp. Western blot analysis of EndoH- or EndoF-treated SARSpp showed that all the S protein in the SARSpp was EndoH resistant and EndoF sensitive, indicating that all the S molecules in SARSpp matured properly (see Fig. 3c).

The transmembrane domain and not the cytoplasmic domain of SARS-CoV S protein is essential for infectivity of SARSpp in VeroE6R cells. Since it was clear from the previous experiments that the SARSpp could be used to test the activity of SARS-CoV S, chimeric S-containing SARSpp were made. We first made sure that the chimeric S SARSpp contained same amounts of S protein as wt-S SARSpp. S-specific immunoprecipitation was carried out on equal amounts (based on the RT assay) of purified radioactively labeled particles. Subsequent SDS-polyacrylamide gel electrophoresis (PAGE) analysis showed (Fig. 4) that chimeric S proteins were incorporated in the pseudotyped particles, at least to the same extent as wt S ($S_{VSV\text{-}TMDCyt}$) or more ($S_{VSV\text{-}Cyt}$ and $S_{MHV\text{-}TMDCyt}$).

VeroE6R cells were infected with equal amounts of particles, and the titers of the chimeric SARSpp were determined and plotted as percentages of the wt SARSpp titer (see Fig. 5). $S_{VSV\text{-}Cyt}$-containing SARSpp, in which the cytoplasmic domain of S was replaced by the cytoplasmic domain of VSV-G, were infectious, up to 40% of wild type. This shows that the cytoplasmic domain of SARS-CoV S is not essential for infectivity, although it appears to have a slightly enhancing effect. In contrast, SARSpp containing $S_{VSV\text{-}TMDCyt}$, the chimera that contains both the TMD and the cytoplasmic domain of VSV-G, were severely impaired in infectivity (<5%). This shows that the TMD of S is somehow involved in the entry process of SARS-CoV. In contrast, SARSpp containing $S_{MHV\text{-}TMDCyt}$, a chimera that contains the TMD and cytoplasmic domain of another coronavirus, MHV A59, were almost as infectious as the particles containing S_{WT} (60%). This indicates that the TMD and cytoplasmic domain of MHV A59 can functionally replace the domains in SARS-CoV.

SARS-CoV S-expressing cells fuse with cells expressing ACE-2. In SARS patients, syncytia in lung tissue have been observed (18). These syncytia are most likely due to the fact that the infected cells express the SARS-CoV spike and the SARS receptor ACE-2 and that interaction between cells expressing these two molecules results in fusion. In contrast with this observation, we were unable to observe any syncytia in VeroE6R cells infected with SARS-CoV (results not shown). We investigated whether the SARS-CoV S protein was able to induce cell-cell fusion in vitro, as has been previously observed by Li et al. (20) by overexpressing ACE-2 and SARS-CoV S. 293T cells were transfected with either pFLACE2/T7rLuc or phCMV-S and pBp9/CMVT7. pFLACE2/T7rLuc encoded CMV promoter-driven ACE-2 and a *Renilla* luciferase gene under a T7 polymerase promoter. In the case of fusion between ACE-2- and S-expressing cells, *Renilla* luciferase could be synthesized. Consequently, the *Renilla* luciferase activity represented the level of cell fusion. Twenty-four hours posttransfection, the cells were mixed and incubated for 17 to 20 h. Microscopic examination of the cells was carried out, and small syncytia were observed (results not shown). Cells were lysed, and the luciferase activities and protein concentrations of the samples were determined.

Figure 6 shows the results obtained with this cell-cell fusion assay. The values of the chimeric S proteins are given relative to that for wt S and are corrected for non-S-related background luciferase activity. Consistent with the results obtained with the SARSpp, $S_{VSV\text{-}Cyt}$ and $S_{MHV\text{-}TMDCyt}$ displayed 50 to 60% of the activity of wt S, indicating that the cytoplasmic domain is not important for fusion and that the TMD and cytoplasmic

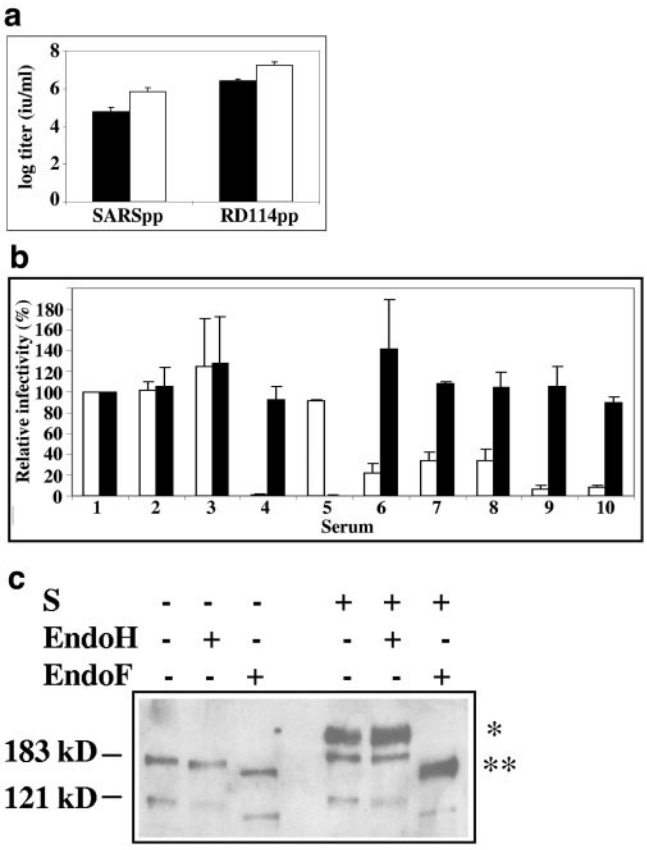

FIG. 3. Characterization of SARSpp. (a) Titer determination of SARS and control pseudotypes. Pseudotypes were prepared as described in Materials and Methods. To determine the titer, VeroE6R cells were transduced and the percentage of GFP-positive cells was determined by FACS. The total amount of GFP-positive cells represented the amount of infectious units (IU), provided that the percentage of positive cells did not exceed 10%. Black bars represent infection without a centrifugation step, and white bars represent infection with a centrifugation step. (b) Neutralization assay with SARS S-specific sera shows that the infectivity of SARSpp is S specific. Prior to titer determination, SARSpp and control RD114pp were incubated with the indicated sera for 45 min. Titers were calculated as for panel a. White bars, SARSpp values; black bars, RD114pp values. Serum numbers: 1, DMEM; 2, normal human serum 640; 3, normal human serum 641; 4, rabbit anti-SARS Marburg University; 5, goat anti-RD114 79S756; 6, human serum Hku 1a; 7, human serum Hku 1b; 8, human serum Hku 2; 9, human serum London; 10, human serum Dellseith. Values are means from three independent experiments. (c) Maturation of S in SARSpp. Maturation of S in the SARSpp was examined by Western blotting of EndoH- or EndoF-treated SARSpp using a rabbit anti-SARS serum for detection. *, EndoH-resistant S; **, S digested by EndoF.

domain of MHV can be used by the SARS-CoV S protein. The result obtained with $S_{VSV\text{-}TMDCyt}$ was remarkably different from the result found with SARSpp $S_{VSV\text{-}TMDCyt}$. The cell-cell fusion value measured for this chimera was around 25%, while the infectivity of $S_{VSV\text{-}TMDCyt}$-containing SARSpp was only about 5% (5 times lower), indicating that the TMD of S is less important for the cell-cell fusion activity than for the infectivity of the SARSpp.

The TMD of SARS-CoV S is less critical for the infectivity of SARSpp in cells expressing human ACE-2 at a high level than

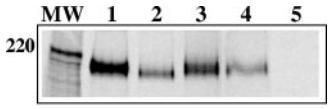

FIG. 4. Incorporation of S chimeras in SARSpp. ^{35}S-labeled SARSpp were purified by centrifugation over a sucrose cushion. The pellets were resuspended, and the concentration of particles was analyzed by the RT assay. Equal amounts of particles were solubilized, and S-specific immunoprecipitation was performed. The samples were run on an 8% PAA gel. Lanes: MW, molecular weight marker; 1, $S_{VSV\text{-}Cyt}$; 2, $S_{VSV\text{-}TMDCyt}$; 3, $S_{MHV\text{-}TMDCyt}$; 4, S_{WT}; 5, mock.

in VeroE6R cells. There are several possible explanations for the difference we observed between the SARSpp assay and the cell-cell fusion assay (see Discussion). One of them is the fact that the ACE-2 molecules in the two assays were not the same: human ACE-2 (cell-cell fusion) versus ACE-2 of the African green monkey (VeroE6R cells in SARSpp assay). Also, the expression levels of ACE-2 may differ in the two assays. The expression level of human ACE-2 in the cell-cell fusion is probably very high, whereas the ACE-2 expression level in VeroE6R cells is lower. It has been shown by Simmons et al. (37) that S-transfected 293T cells do not fuse with VeroE6 cells. Therefore, we decided to use the 293T cells transiently expressing ACE-2 in the SARSpp assay in order to be able to fairly compare cell-cell fusion activity and SARSpp infectivity. Transduction of the ACE-2-transfected cells was carried out 24 h posttransfection, and GFP expression was measured 72 h posttransduction. Figure 7 shows the relative infectivity of the SARSpp containing S chimeras compared to the wild type. The dramatic lack of infectivity of the $S_{VSV\text{-}TMDCyt}$ SARSpp, as observed with VeroE6R cells, was less pronounced in the ACE-2-transfected cells (3 versus 10% relative infectivity). However, the influence of the TMD and cytoplasmic domain of VSV-G on infectivity was still quite substantial. In addition, the SARSpp displaying one of the other two chimeras, $S_{VSV\text{-}Cyt}$ and $S_{MHV\text{-}TMDCyt}$, had a much higher infectivity than wild-type S-containing SARSpp. In summary, the influence of the TMD on infectivity is more pronounced than that on cell-cell fusion.

The TMD of SARS-CoV S is important for S trimer stability. It has been shown before that SARS-CoV S oligomerizes into dimers and trimers (39, 39, 46, 52). We investigated the oligomeric state of the S chimeras $S_{VSV\text{-}Cyt}$, $S_{VSV\text{-}TMDCyt}$, and $S_{MHV\text{-}TMDCyt}$ in the SARSpp by immunoprecipitation of S after purification of SARSpp. Samples were run on SDS-PAGE (4%) gels under

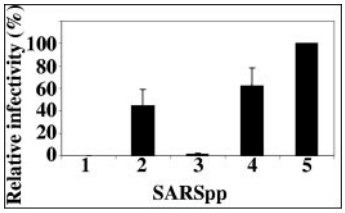

FIG. 5. Infectivity of SARSpp chimeras. SARSpp containing S or chimeric S were produced by 293T cells, and the titers were determined on Vero E6R cells as for Fig. 3. Titers of the chimeric S-containing pseudoparticles are shown as percentages of wild-type S-containingpseudoparticles.Columns:1,mock;2,$S_{VSV\text{-}Cyt}$;3,$S_{VSV\text{-}TMDCyt}$; 4, $S_{MHV\text{-}TMDCyt}$; 5, S_{WT}.

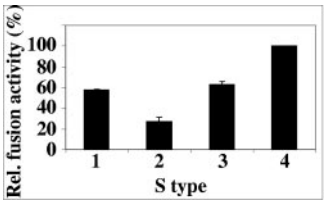

FIG. 6. Fusogenicity of S chimeras as determined by the cell-cell fusion assay. Fusion activity of the S chimeras was determined using the *Renilla* luciferase-based cell-cell fusion assay. *Renilla* activity of cell lysates was determined and corrected for the protein concentration. Subsequently, the background (S-independent rLuc activity) was subtracted and the remaining activity was plotted as a percentage of the wild type level. Columns: 1, $S_{VSV\text{-}Cyt}$; 2, $S_{VSV\text{-}TMDCyt}$; 3, $S_{MHV\text{-}TMDCyt}$; 4, S_{WT}.

nonreducing conditions, with half of the sample being incubated at 80°C and the other half at room temperature. The results are shown in Fig. 8. When the samples were not heated, a smear of protein bands was visible, probably representing the heterogeneity of glycosylation of S. After incubation of the sample for 5 min at 80°C (39), three distinctive bands, most likely representing S trimers, dimers, and monomers, were visible for wt S and all three chimeras. However, the ratio between the three forms in $S_{VSV\text{-}TMDCyt}$ differed from the ratio observed in S_{WT} and the two other chimeras. Quantification of the bands by phosphorimaging and Quantityone software (Bio-Rad) showed that the percentage of trimers of $S_{VSV\text{-}TMDCyt}$ is only half of the percentage of trimers seen in the other three samples, suggesting that the $S_{VSV\text{-}TMDCyt}$ trimers were less stable at 80°C than wt S protein. Moreover, Fig. 2b showed an extra S-specific band, most likely an S oligomer. Also on this blot, the $S_{VSV\text{-}TMDCyt}$ oligomer band is weaker than the oligomer band in the other lanes. Since $S_{VSV\text{-}TMDCyt}$ contains the TMD of VSV-G, this result suggests that the coronavirus S TMD is involved in stabilization of the S trimer.

DISCUSSION

The entry of SARS-CoV is an essential step in the viral life cycle. It is evident that the S protein is crucial in this process. It binds to the cellular receptor, and it is responsible for fusion of the viral and cell membranes, giving the viral RNA access to the cytosol.

In this paper, the role of the strongly conserved transmembrane domain of SARS-CoV in virus entry has been investi-

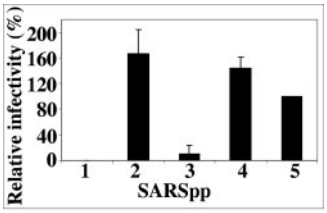

FIG. 7. SARSpp infectivity in 293T cells transfected with human ACE-2. 293T cells were transfected with pFLACE2/T7rLuc. Twenty-four hours later, the cells were transduced with SARSpp and incubated for 3 days. Transduced cells were scored by FACS analysis, and the infectivity of the chimeric S-containing SARSpp was plotted as a percentage of that of wild-type S-containing SARSpp. Columns: 1, mock; 2, $S_{VSV\text{-}Cyt}$; 3, $S_{VSV\text{-}TMDCyt}$; 4, $S_{MHV\text{-}TMDCyt}$; 5, S_{WT}.

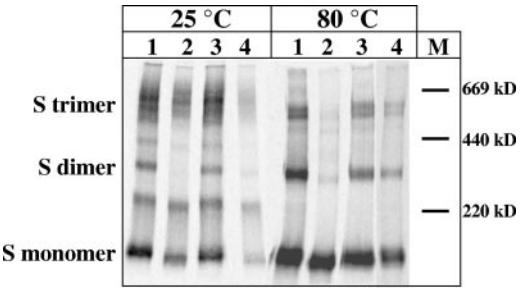

FIG. 8. Examination of the oligomeric state of S in SARSpp. ^{35}S-labeled SARSpp were concentrated through a sucrose cushion, and the particles were resuspended. Half of the sample was subjected to an 80°C incubation step. Both treated and untreated samples were run on a 4% polyacrylamide gel under nonreducing conditions and were made visible by phosphorimaging. S monomers, dimers, and trimers are indicated, as are the marker bands. Lanes: 1, $S_{VSV\text{-}Cyt}$; 2, $S_{VSV\text{-}TMDCyt}$; 3, $S_{MHV\text{-}TMDCyt}$; 4, S_{WT}.

gated by making use of the MLV-based pseudotyping system. This system has been proven to be a valuable tool for studying the functions of viral glycoproteins. In addition, it is a safe system for study of the cell entry of human viruses that can be lethal and therefore should be cultured in highly restricted laboratories. Cell-cell fusion activity of SARS-CoV S was also measured. As an alternative approach to score for syncytium formation by microscopic determination, we developed an assay based on T7-driven luciferase activity to quantify the extent of cell fusion.

Transfection of 293T cells with phCMV-S_{WT} readily resulted in expression of S that could be measured by immunofluorescence (results not shown) and immunoprecipitation (Fig. 2). Previously, Simmons et al. have reported that CMV promoter-driven expression of SARS-CoV S failed to give detectable levels of S (37). Others have reported that expression of S from the CMV promoter was detectable only after codon optimization (25, 28). Clearly, in our hands, using a CMV promoter to express SARS-CoV S was no problem. This could be related to the strain of virus used but could also be due to the phCMV plasmid, in which a splicing signal has been cloned upstream of the S-encoding sequence, thereby making a more stable mRNA (25).

SARSpp were able to infect SARS-CoV-permissive cells, and infection with these particles was S specific, as evidenced by inhibition with anti-SARS-CoV antibodies (Fig. 3b). The titers of the SARSpp reached levels (10^5 to 10^6) previously described by one other group only (16). Other reports have shown much lower titers (13, 25, 37). In addition, no assays have been described in which the cell-cell fusion activity of SARS-CoV was measured in a quantitative way. Here cell-cell fusion mediated by SARS-CoV S and ACE-2 was detected using the luciferase-based assay. No cell-cell fusion was observed in the absence of ACE-2 or S (data not shown). Microscopic investigation of the mixed, transfected 293T cells showed that the extent of cell-cell fusion does not compare with that seen in MHV-infected cells, which gives rise to massive syncytium formation (3). Rather, in our SARS S-driven experiments, we could see small groups of cells fused together. We did not observe any syncytium formation during SARS-CoV infection of VeroE6R cells, whereas Ksiazek et al. reported that syncytia could be ob-

served in infected lung tissue (18). It is unclear why syncytium formation is observed only in particular cases. It might be related to the level of ACE-2 and S expression or to the lower affinity of the African green monkey ACE-2 for the S protein. Indeed, recent results have shown that a change of only a few residues in ACE-2 can result in a great difference in affinity for SARS-CoV S (21). Possibly, other factors might be involved, such as the need for a coreceptor.

Replacement of the S cytoplasmic domain with the VSV-G cytoplasmic domain had a mild effect on the activity of S both in the SARSpp assay and in the cell-cell fusion assay. This confirms a previous report on MHV fusion, based on syncytium formation, in which it was shown that the VSV-G cytoplasmic tail can replace the S tail without inhibiting fusion activity (3).

The $S_{MHV\text{-}TMDCyt}$ chimera, in which the SARS-CoV S TMD and cytoplasmic domain have been replaced by those originating from MHV, shows fusion activity with a slight reduction (50 to 60% activity). This shows that the TMD of MHV can serve as a membrane anchor for SARS-CoV S. Clearly, the strong sequence conservation of the coronavirus S TMD ensures that its function is also conserved.

When both the TMD and cytoplasmic tail of S were replaced with those of VSV-G, a remarkable reduction in fusion activity was observed in the SARSpp assay, using VeroE6R cells, resulting in <5% activity. This shows the importance of the TMD for SARSpp entry into VeroE6R cells. However, the cell-cell fusion assay showed a different result. There was 20 to 30% activity in this assay, showing a significant discrepancy between the two assays. By using ACE-2-transfected 293T cells instead of VeroE6R cells in the SARSpp assay, the $S_{VSV\text{-}TMDCyt}$ chimera exhibited 10% activity. The reason for the difference in infectivity between the two cell lines may be found in the difference in receptor expression level and affinity (human versus African green monkey ACE-2), which may result in a changed fusion activity. Another reason might be that the TMD is less important for S-mediated cell-cell fusion than for S-mediated infectivity.

Based on the three experiments described here, we conclude that $S_{VSV\text{-}TMDCyt}$ has a significantly lower activity than wild-type S. We and others have reported earlier that the Cys-rich domain of the TMD is important for fusion (3, 5), which might explain the lowered activity of the $S_{VSV\text{-}TMDCyt}$ chimera, lacking the Cys-rich domain. Also, the highly conserved Trp-rich domain is not present in the $S_{VSV\text{-}TMDCyt}$ chimera, which might be an additional explanation for the lowered activity of $S_{VSV\text{-}TMDCyt}$. Another possible explanation for lowered $S_{VSV\text{-}TMDCyt}$ activity may be the lower stability of the $S_{VSV\text{-}TMDCyt}$ trimer. It has been suggested before that the oligomeric state of S may be important for fusion activity (22). At this point we do not know if the stability of S trimers is directly linked to membrane fusion activity, but this interesting option cannot be ruled out at this time.

As mentioned before, the TMD of coronaviruses is highly conserved. It consists of a N-terminal tryptophan-rich domain, a central hydrophobic domain, and a C-terminal cysteine-rich domain. A tryptophan-rich domain, located close to the TMD of HIV gp41, has been described to be important for HIV fusion (35), in particular on the level of pore dilation (26). Since we do not know where exactly the TMD of SARS-CoV S starts, it could be that the tryptophan-rich domain of coronavirus S in fact precedes the actual transmembrane part and that this domain can partition into interfacial regions of membranes, as has been described for the Trp-rich juxtamembrane domain in gp41 and has been proposed to occur in viral fusion proteins in other virus families through regions enriched in aromatic residues (29, 41). Moreover, a recent study on SARS-CoV S has identified the "pretransmembrane" region (i.e., the Trp-rich domain) as a membrane-active region, possibly involved in membrane fusion, in analogy with the HIV gp41 Trp-rich domain (14). In addition, Sainz et al. (33) propose that the coronavirus S Trp-rich region, after the HR six-helix bundle has formed, aligns with the fusion peptide, thus creating an extended hydrophobic stretch that aids the lipid flow, thereby establishing a fusion pore. Finally, it has been suggested that the Trp-rich region in gp41 might also be involved in prefusion trimerization (31), which might be related to the S trimerization and the $S_{VSV\text{-}TMDCyt}$ trimer instability we observed.

The cysteine-rich domain has been shown to be necessary for fusion of MHV, as evidenced by mutational analysis (3, 5). Some of these Cys residues are palmitoylated, arguing for a strong membrane association (3), although it is not clear whether this region is located within the membrane. It has been shown that the cysteine residues are involved in the transition from hemifusion to fusion during MHV-S-mediated cell-cell fusion (5), a situation reminiscent of the role that acylated cysteine residues have been described to play in influenza virus hemagglutinin-mediated membrane fusion (34). In addition, for MHV, deletion of three of the seven cysteines in the TMD results in a defect in cell-cell fusion but not in virus-cell fusion (50). Despite these reported effects of the cysteine residues on the membrane fusion activity of coronavirus S proteins, there is no model by which the mode of action of these residues during fusion can be explained.

To better understand the membrane fusion process of SARS-CoV, we are currently further investigating the function of these Trp-rich and Cys-rich domains in SARS-CoV S.

ACKNOWLEDGMENTS

We thank A. D. M. E. Osterhaus for VeroE6R cells, H. W. Doerr, H. F. Rabenau, and M. Niedrig for antisera, P. Bredenbeek for critical reading of the manuscript, D. van Leeuwen for assistance with the biotinylation experiment and FACS, O. Slobodskaya for assistance with FACS, H. van Leeuwen for pBp9/CMVT7, C. Reusken for pHCVwt-RLuc-3′UTR, and E. Snijder and J. Zevenhoven-Dobbe for initial cloning and sequencing of the spike construct.

This work was supported by "Agence Nationale pour la Recherche sur le SIDA et les Hépatites Virales" (ANRS), the European Community (COMPUVAC LSHB-CT-2004-005246), Région Rhône-Alpes, and Ligue Nationale Contre le Cancer.

REFERENCES

1. **Babcock, G. J., D. J. Esshaki, W. D. Thomas, Jr., and D. M. Ambrosino.** 2004. Amino acids 270 to 510 of the severe acute respiratory syndrome coronavirus spike protein are required for interaction with receptor. J. Virol. **78:**4552–4560.
2. **Bartosch, B., J. Dubuisson, and F. L. Cosset.** 2003. Infectious hepatitis C virus pseudo-particles containing functional E1–E2 envelope protein complexes. J. Exp. Med. **197:**633–642.
3. **Bos, E. C., L. Heijnen, W. Luytjes, and W. J. Spaan.** 1995. Mutational analysis of the murine coronavirus spike protein: effect on cell-to-cell fusion. Virology **214:**453–463.
4. **Bosch, B. J., R. van der Zee, C. A. M. de Haan, and P. J. M. Rottier.** 2003. The coronavirus spike protein is a class I virus fusion protein: structural and functional characterization of the fusion core complex. J. Virol. **77:**8801–8811.

5. **Chang, K. W., Y. Sheng, and J. L. Gombold.** 2000. Coronavirus-induced membrane fusion requires the cysteine-rich domain in the spike protein. Virology **269:**212–224.
6. **Colman, P. M., and M. C. Lawrence.** 2003. The structural biology of type I viral membrane fusion. Nat. Rev. Mol. Cell Biol. **4:**309–319.
7. **Davanloo, P., A. H. Rosenberg, J. J. Dunn, and F. W. Studier.** 1984. Cloning and expression of the gene for bacteriophage T7 RNA polymerase. Proc. Natl. Acad. Sci. USA **81:**2035–2039.
8. **de Groot, R. J., W. Luytjes, M. C. Horzinek, B. A. van der Zeijst, W. J. Spaan, and J. A. Lenstra.** 1987. Evidence for a coiled-coil structure in the spike proteins of coronaviruses. J. Mol. Biol. **196:**963–966.
9. **Delmas, B., and H. Laude.** 1990. Assembly of coronavirus spike protein into trimers and its role in epitope expression. J. Virol. **64:**5367–5375.
10. **Drosten, C., S. Gunther, W. Preiser, S. van der Werf, H. R. Brodt, S. Becker, H. Rabenau, M. Panning, L. Kolesnikova, R. A. Fouchier, A. Berger, A. M. Burguiere, J. Cinatl, M. Eickmann, N. Escriou, K. Grywna, S. Kramme, J. C. Manuguerra, S. Muller, V. Rickerts, M. Sturmer, S. Vieth, H. D. Klenk, A. D. Osterhaus, H. Schmitz, and H. W. Doerr.** 2003. Identification of a novel coronavirus in patients with severe acute respiratory syndrome. N. Engl. J. Med. **348:**1967–1976.
11. **Frana, M. F., J. N. Behnke, L. S. Sturman, and K. V. Holmes.** 1985. Proteolytic cleavage of the E2 glycoprotein of murine coronavirus: host-dependent differences in proteolytic cleavage and cell fusion. J. Virol. **56:**912–920.
12. **Gallagher, T. M., and M. J. Buchmeier.** 2001. Coronavirus spike proteins in viral entry and pathogenesis. Virology **279:**371–374.
13. **Giroglou, T., J. Cinatl, Jr., H. Rabenau, C. Drosten, H. Schwalbe, H. W. Doerr, and D. von Laer.** 2004. Retroviral vectors pseudotyped with severe acute respiratory syndrome coronavirus S protein. J. Virol. **78:**9007–9015.
14. **Guillen, J., A. J. Perez-Berna, M. R. Moreno, and J. Villalain.** 2005. Identification of the membrane-active regions of the severe acute respiratory syndrome coronavirus spike membrane glycoprotein using a 16/18-mer peptide scan: implications for the viral fusion mechanism. J. Virol. **79:**1743–1752.
15. **Hamming, I., W. Timens, M. L. Bulthuis, A. T. Lely, G. J. Navis, and H. van Goor.** 2004. Tissue distribution of ACE2 protein, the functional receptor for SARS coronavirus. A first step in understanding SARS pathogenesis. J. Pathol. **203:**631–637.
16. **Hofmann, H., K. Hattermann, A. Marzi, T. Gramberg, M. Geier, M. Krumbiegel, S. Kuate, K. Uberla, M. Niedrig, and S. Pohlmann.** 2004. S protein of severe acute respiratory syndrome-associated coronavirus mediates entry into hepatoma cell lines and is targeted by neutralizing antibodies in infected patients. J. Virol. **78:**6134–6142.
17. **Jeffers, S. A., S. M. Tusell, L. Gillim-Ross, E. M. Hemmila, J. E. Achenbach, G. J. Babcock, W. D. Thomas, Jr., L. B. Thackray, M. D. Young, R. J. Mason, D. M. Ambrosino, D. E. Wentworth, J. C. Demartini, and K. V. Holmes.** 2004. CD209L (L-SIGN) is a receptor for severe acute respiratory syndrome coronavirus. Proc. Natl. Acad. Sci. USA **101:**15748–15753.
18. **Ksiazek, T. G., D. Erdman, C. S. Goldsmith, S. R. Zaki, T. Peret, S. Emery, S. X. Tong, C. Urbani, J. A. Comer, W. Lim, P. E. Rollin, S. F. Dowell, A. E. Ling, C. D. Humphrey, W. J. Shieh, J. Guarner, C. D. Paddock, P. Rota, B. Fields, J. DeRisi, J. Y. Yang, N. Cox, J. M. Hughes, J. W. Leduc, W. J. Bellini, and L. J. Anderson.** 2003. A novel coronavirus associated with severe acute respiratory syndrome. N. Engl. J. Med. **348:**1953–1966.
19. **Laemmli, U. K.** 1970. Cleavage of structural proteins during the assembly of the head of bacteriophage T4. Nature **227:**680–685.
20. **Li, W., M. J. Moore, N. Vasilieva, J. Sui, S. K. Wong, M. A. Berne, M. Somasundaran, J. L. Sullivan, K. Luzuriaga, T. C. Greenough, H. Choe, and M. Farzan.** 2003. Angiotensin-converting enzyme 2 is a functional receptor for the SARS coronavirus. Nature **426:**450–454.
21. **Li, W., C. Zhang, J. Sui, J. H. Kuhn, M. J. Moore, S. Luo, S. K. Wong, I. C. Huang, K. Xu, N. Vasilieva, A. Murakami, Y. He, W. A. Marasco, Y. Guan, H. Choe, and M. Farzan.** 2005. Receptor and viral determinants of SARS-coronavirus adaptation to human ACE2. EMBO J. **24:**1634–1643.
22. **Luo, Z., A. M. Matthews, and S. R. Weiss.** 1999. Amino acid substitutions within the leucine zipper domain of the murine coronavirus spike protein cause defects in oligomerization and the ability to induce cell-to-cell fusion. J. Virol. **73:**8152–8159.
23. **Marra, M. A., S. J. M. Jones, C. R. Astell, R. A. Holt, A. Brooks-Wilson, Y. S. N. Butterfield, J. Khattra, J. K. Asano, S. A. Barber, S. Y. Chan, A. Cloutier, S. M. Coughlin, D. Freeman, N. Girn, O. L. Griffin, S. R. Leach, M. Mayo, H. McDonald, S. B. Montgomery, P. K. Pandoh, A. S. Petrescu, A. G. Robertson, J. E. Schein, A. Siddiqui, D. E. Smailus, J. E. Stott, G. S. Yang, F. Plummer, A. Andonov, H. Artsob, N. Bastien, K. Bernard, T. F. Booth, D. Bowness, M. Czub, M. Drebot, L. Fernando, R. Flick, M. Garbutt, M. Gray, A. Grolla, S. Jones, H. Feldmann, A. Meyers, A. Kabani, Y. Li, S. Normand, U. Stroher, G. A. Tipples, S. Tyler, R. Vogrig, D. Ward, B. Watson, R. C. Brunham, M. Krajden, M. Petric, D. M. Skowronski, C. Upton, and R. L. Roper.** 2003. The genome sequence of the SARS-associated coronavirus. Science **300:**1399–1404.
24. **Marzi, A., T. Gramberg, G. Simmons, P. Moller, A. J. Rennekamp, M. Krumbiegel, M. Geier, J. Eisemann, N. Turza, B. Saunier, A. Steinkasserer, S. Becker, P. Bates, H. Hofmann, and S. Pohlmann.** 2004. DC-SIGN and DC-SIGNR interact with the glycoprotein of Marburg virus and the S protein of severe acute respiratory syndrome coronavirus. J. Virol. **78:**12090–12095.
25. **Moore, M. J., T. Dorfman, W. Li, S. K. Wong, Y. Li, J. H. Kuhn, J. Coderre, N. Vasilieva, Z. Han, T. C. Greenough, M. Farzan, and H. Choe.** 2004. Retroviruses pseudotyped with the severe acute respiratory syndrome coronavirus spike protein efficiently infect cells expressing angiotensin-converting enzyme 2. J. Virol. **78:**10628–10635.
26. **Munoz-Barroso, I., K. Salzwedel, E. Hunter, and R. Blumenthal.** 1999. Role of the membrane-proximal domain in the initial stages of human immunodeficiency virus type 1 envelope glycoprotein-mediated membrane fusion. J. Virol. **73:**6089–6092.
27. **Negre, D., P. E. Mangeot, G. Duisit, S. Blanchard, P. O. Vidalain, P. Leissner, A. J. Winter, C. Rabourdin-Combe, M. Mehtali, P. Moullier, J. L. Darlix, and F. L. Cosset.** 2000. Characterization of novel safe lentiviral vectors derived from simian immunodeficiency virus (SIVmac251) that efficiently transduce mature human dendritic cells. Gene Ther. **7:**1613–1623.
28. **Nie, Y., P. Wang, X. Shi, G. Wang, J. Chen, A. Zheng, W. Wang, Z. Wang, X. Qu, M. Luo, L. Tan, X. Song, X. Yin, J. Chen, M. Ding, and H. Deng.** 2004. Highly infectious SARS-CoV pseudotyped virus reveals the cell tropism and its correlation with receptor expression. Biochem. Biophys. Res. Commun. **321:**994–1000.
29. **Nieva, J. L., and T. Suarez.** 2000. Hydrophobic-at-interface regions in viral fusion protein ectodomains. Biosci. Rep. **20:**519–533.
30. **Peiris, J. S. M., S. T. Lai, L. L. M. Poon, Y. Guan, L. Y. C. Yam, W. Lim, J. Nicholls, W. K. S. Yee, W. W. Yan, M. T. Cheung, V. C. C. Cheng, K. H. Chan, D. N. C. Tsang, R. W. H. Yung, T. K. Ng, and K. Y. Yuen.** 2003. Coronavirus as a possible cause of severe acute respiratory syndrome. Lancet **361:**1319–1325.
31. **Saez-Cirion, A., J. L. Arrondo, M. J. Gomara, M. Lorizate, I. Iloro, G. Melikyan, and J. L. Nieva.** 2003. Structural and functional roles of HIV-1 gp41 pretransmembrane sequence segmentation. Biophys. J. **85:**3769–3780.
32. **Sainz, B., Jr., J. M. Rausch, W. R. Gallaher, R. F. Garry, and W. C. Wimley.** 2005. Identification and characterization of the putative fusion peptide of the severe acute respiratory syndrome-associated coronavirus spike protein. J. Virol. **79:**7195–7206.
33. **Sainz, B., Jr., J. M. Rausch, W. R. Gallaher, R. F. Garry, and W. C. Wimley.** 2005. The aromatic domain of the coronavirus class I viral fusion protein induces membrane permeabilization: putative role during viral entry. Biochemistry **44:**947–958.
34. **Sakai, T., R. Ohuchi, and M. Ohuchi.** 2002. Fatty acids on the A/USSR/77 influenza virus hemagglutinin facilitate the transition from hemifusion to fusion pore formation. J. Virol. **76:**4603–4611.
35. **Salzwedel, K., J. T. West, and E. Hunter.** 1999. A conserved tryptophan-rich motif in the membrane-proximal region of the human immunodeficiency virus type 1 gp41 ectodomain is important for Env-mediated fusion and virus infectivity. J. Virol. **73:**2469–2480.
36. **Simmons, G., D. N. Gosalia, A. J. Rennekamp, J. D. Reeves, S. L. Diamond, and P. Bates.** 2005. Inhibitors of cathepsin L prevent severe acute respiratory syndrome coronavirus entry. Proc. Natl. Acad. Sci. USA **102:**11876–11881.
37. **Simmons, G., J. D. Reeves, A. J. Rennekamp, S. M. Amberg, A. J. Piefer, and P. Bates.** 2004. Characterization of severe acute respiratory syndrome-associated coronavirus (SARS-CoV) spike glycoprotein-mediated viral entry. Proc. Natl. Acad. Sci. USA **101:**4240–4245.
38. **Snijder, E. J., P. J. Bredenbeek, J. C. Dobbe, V. Thiel, J. Ziebuhr, L. L. Poon, Y. Guan, M. Rozanov, W. J. Spaan, and A. E. Gorbalenya.** 2003. Unique and conserved features of genome and proteome of SARS-coronavirus, an early split-off from the coronavirus group 2 lineage. J. Mol. Biol. **331:**991–1004.
39. **Song, H. C., M. Y. Seo, K. Stadler, B. J. Yoo, Q. L. Choo, S. R. Coates, Y. Uematsu, T. Harada, C. E. Greer, J. M. Polo, P. Pileri, M. Eickmann, R. Rappuoli, S. Abrignani, M. Houghton, and J. H. Han.** 2004. Synthesis and characterization of a native, oligomeric form of recombinant severe acute respiratory syndrome coronavirus spike glycoprotein. J. Virol. **78:**10328–10335.
40. **Sturman, L. S., C. S. Ricard, and K. V. Holmes.** 1985. Proteolytic cleavage of the E2 glycoprotein of murine coronavirus: activation of cell-fusing activity of virions by trypsin and separation of two different 90K cleavage fragments. J. Virol. **56:**904–911.
41. **Suarez, T., W. R. Gallaher, A. Agirre, F. M. Goni, and J. L. Nieva.** 2000. Membrane interface-interacting sequences within the ectodomain of the human immunodeficiency virus type 1 envelope glycoprotein: putative role during viral fusion. J. Virol. **74:**8038–8047.
42. **Supekar, V. M., C. Bruckmann, P. Ingallinella, E. Bianchi, A. Pessi, and A. Carfi.** 2004. Structure of a proteolytically resistant core from the severe acute respiratory syndrome coronavirus S2 fusion protein. Proc. Natl. Acad. Sci. USA **101:**17958–17963.
43. **Vennema, H., R. Rijnbrand, L. Heijnen, M. C. Horzinek, and W. J. Spaan.** 1991. Enhancement of the vaccinia virus/phage T7 RNA polymerase expression system using encephalomyocarditis virus 5′-untranslated region sequences. Gene **108:**201–209.
44. **Wong, S. K., W. Li, M. J. Moore, H. Choe, and M. Farzan.** 2004. A 193-

amino acid fragment of the SARS coronavirus S protein efficiently binds angiotensin-converting enzyme 2. J. Biol. Chem. **279:**3197–3201.

45. **Xiao, X., S. Chakraborti, A. S. Dimitrov, K. Gramatikoff, and D. S. Dimitrov.** 2003. The SARS-CoV S glycoprotein: expression and functional characterization. Biochem. Biophys. Res. Commun. **312:**1159–1164.
46. **Xiao, X., Y. Feng, S. Chakraborti, and D. S. Dimitrov.** 2004. Oligomerization of the SARS-CoV S glycoprotein: dimerization of the N-terminus and trimerization of the ectodomain. Biochem. Biophys. Res. Commun. **322:**93–99.
47. **Xu, Y., Y. Liu, Z. Lou, L. Qin, X. Li, Z. Bai, H. Pang, P. Tien, G. F. Gao, and Z. Rao.** 2004. Structural basis for coronavirus-mediated membrane fusion. Crystal structure of mouse hepatitis virus spike protein fusion core. J. Biol. Chem. **279:**30514–30522.
48. **Xu, Y., Z. Lou, Y. Liu, H. Pang, P. Tien, G. F. Gao, and Z. Rao.** 2004. Crystal structure of severe acute respiratory syndrome coronavirus spike protein fusion core. J. Biol. Chem. **279:**49414–49419.
49. **Yang, Z. Y., Y. Huang, L. Ganesh, K. Leung, W. P. Kong, O. Schwartz, K. Subbarao, and G. J. Nabel.** 2004. pH-dependent entry of severe acute respiratory syndrome coronavirus is mediated by the spike glycoprotein and enhanced by dendritic cell transfer through DC-SIGN. J. Virol. **78:**5642–5650.
50. **Ye, R., C. Montalto-Morrison, and P. S. Masters.** 2004. Genetic analysis of determinants for spike glycoprotein assembly into murine coronavirus virions: distinct roles for charge-rich and cysteine-rich regions of the endodomain. J. Virol. **78:**9904–9917.
51. **Zelus, B. D., J. H. Schickli, D. M. Blau, S. R. Weiss, and K. V. Holmes.** 2003. Conformational changes in the spike glycoprotein of murine coronavirus are induced at 37 degrees C either by soluble murine CEACAM1 receptors or by pH 8. J. Virol. **77:**830–840.
52. **Zhou, T., H. Wang, D. Luo, T. Rowe, Z. Wang, R. J. Hogan, S. Qiu, R. J. Bunzel, G. Huang, V. Mishra, T. G. Voss, R. Kimberly, and M. Luo.** 2004. An exposed domain in the severe acute respiratory syndrome coronavirus spike protein induces neutralizing antibodies. J. Virol. **78:**7217–7226.